

# Fast Glioblastoma Detection in Fluid-attenuated inversion recovery (FLAIR) images by Topological Explainable Automatic Machine Learning

Matteo Rucco<sup>\*1</sup>, Giovanna Viticchi - MD<sup>2</sup>, and Lorenzo Falsetti -  
MD PhD<sup>3</sup>

<sup>1</sup>United Technology Research Center, Via Praga 5, 38121 Trento  
(Tn), Italy.

<sup>2</sup>Neurological Clinic, Marche Polytechnic University, Ancona (An),  
Italy

<sup>3</sup>Internal and Sub-intensive Medicine Department, A.O.U. "Ospedali  
Riuniti", Ancona, Italy

## Abstract

Glioblastoma multiforme (GBM) is a fast-growing and highly invasive brain tumor, it tends to occur in adults between the ages of 45 and 70 and it accounts for 52 percent of all primary brain tumors. Usually, GBMs are detected by magnetic resonance images (MRI). Among MRI images, Fluid-attenuated inversion recovery (FLAIR) sequence produces high quality digital tumor representation. Fast detection and segmentation techniques are needed for overcoming subjective medical doctors (MDs) judgment. In this work, a new framework for radiomics analysis of GBM on FLAIR images is proposed. The framework can be used both for a fast "negative or positive" detection of GBM and eventually for its segmentation. The novelty of the methodology is the combination of new topological features computed by topological data analysis, textural features and of automatic interpretable machine learning algorithm. The framework was evaluated on a public available dataset and it reaches up to the 97% of accuracy on the detection task and up to 95% of accuracy on the segmentation task.

---

<sup>\*</sup>Corresponding Author: [matteo.rucco@utrc.utc.com](mailto:matteo.rucco@utrc.utc.com)

**Keywords** Glioblastoma; Fluid-attenuated inversion recovery; Brain; Tumor; Topological Data Analysis; Persistent Homology; Persistent Entropy; Interpretable Machine Learning; Explainable Machine Learning; Automatic Machine Learning; Co-occurrence matrix; Textural features; The Cancer Imaging Archive

## 1 Introduction

Gliomas are the most common primary brain tumors, originating from glial cells. We can differentiate between benign tumors, with in some cases a lifelong expectancy, and malignant forms. In this second group, glioblastoma multiforme (GBM) is the most frequent malignant cancer with the worst prognosis, with less than 5% of affected patients with a 5-year survival rate and with the highest relapse rate [5]. GBM are characterized by a diffuse and infiltrative growth pattern, as invasive glioma cells often migrate along myelinated white matter (WM) fiber tracts. This is a major cause of their appalling prognosis: tumor cells invade, displace, and possibly destroy WM. For these reasons, surgical, radiotherapeutic and chemotherapeutic approaches, also early performed, rarely resulted effective for a significant number of months [52]. Moreover, large surgical resections could cause unacceptable effects on motor or speech functions. In largely infiltrative GBM the real objective of surgical approach is to leave less possible cancer cells in situ to give more chances to adjuvant therapy. The non-invasive detection of microscopic infiltrations, as well as the identification of aggressive tumor components within spatially heterogeneous lesions, are of outstanding importance for surgical and radiation therapy planning or to assess response to chemotherapy. Moreover, the critical importance of an accurate detection of local infiltration is underlined by the results of intraoperative MR: this technique seems to be able to contribute significantly to optimal resection [28] and to improve post-operative outcomes [45]. Magnetic resonance (MR) imaging plays an important role in the detection and evaluation of brain tumors. The evaluation of post-surgical residual cancer by MR should be performed in all patients after 48-72 hours after surgery, because this factor has a relevant prognostic value both for survival and for the subsequent therapeutic response [31]. For more than 30 years [15] conventional MR imaging, typically T1w images before and after paramagnetic contrast administration, T2w images and FLAIR images have been largely used to evaluate brain neoplasms. MR allows to localize the lesions, helps to distinguish tumors from other pathologic processes, and depicts basic signs of response to therapy, such as changes in size and degree of contrast enhancement. Manual tumor detection and segmentation on MR images is time-consuming and can have a great interobserver variability; automatic segmentation is more reproducible and efficient when robustness is particularly desirable, such as in

monitoring disease progression or in the longitudinal evaluation of emerging therapies [10]. This is a very relevant element because often in clinical practice the decisions regarding therapy continuation or discontinuation are taken on the basis of disease recovery. [52] Radiomics is a set of techniques for extracting a vectorial representation that provides a quantitative description of tumor radiographic data. In general, radiomics extracts quantitative description of signals and images intensity, texture description and geometric characteristics. Texture analysis, an image-analysis technique that quantifies gray-level patterns by describing the statistical relationships between the intensity of pixels, has demonstrated considerable potential for cerebral lesion characterization and segmentation [11, 39, 44]. For automatic glioma detection and segmentation in MRI, several algorithms have been already proposed. The most recent works can be grouped into superpixel based segmentation and deep learning based segmentation. In [55], the authors presented an interesting bottom-up approach that aims to combine graphical probabilistic model (i. e., Conditional Random Fields - CRF -) for capturing the spatial interactions among image superpixel regions and their measurements. A number of features including statistics features, the combined features from the local binary pattern as well as gray level run length, curve features, and fractal features were extracted from each superpixel. The features were used for teaching machine learning models to discriminate between healthy and pathological brain tissues. In [53], the authors used the concept of superpixels based segmentation for instrumenting a machine learning algorithm (i.e., support vector machine - SVM) that uses both textural and statistical features. The authors reported excellent average Dice coefficient, Hausdorff distance, sensitivity, and specificity scores when applying their method on T2w sequences from the Multimodal Brain Tumor Image Segmentation Benchmark 2017 (BraTS2017) dataset. In [48], the authors exploited a new method for brain tumor detection by combining features computed from Fluid-Attenuated Inversion Recovery (flair) MRI in association with the graph-based manifold ranking algorithm. The algorithm counts three main steps: in the first phase, superpixel method is used to convert the homogeneous pixels in the form of superpixels. Rank of each superpixel or node is computed based on the affinity against certain selected nodes as the background prior in the second phase. The relevance of each node with the background prior is then computed and represented in the form of tumor map. In [49] the authors have reported on an approach that computes for each superpixel a number of novel image features including intensity-based, Gabor textures, fractal analysis and curvatures within the entire brain area in FLAIR MRI to ensure a robust classification. The authors compared Extremely randomized trees (ERT) classifier with support vector machine (SVM) to classify each superpixel into tumour and non-tumour. Deep learning based solutions

are becoming the new tools for brain segmentation. In [27], the authors used autoencoders for instrumenting an automatic segmentation of increased signal regions in fluid-attenuated inversion recovery magnetic resonance imaging images. In [30], the authors have provided a solution for dealing to the limited amount of available data from ill brains. They have trained a one-class classifier algorithm based on deep learning for segmenting brain tumors from fluid attenuation inversion recovery MRI. The technique exploits fully convolutional neural networks, and it is equipped with a battery of augmentation techniques that make the algorithm robust against low data quality, and heterogeneity of small training sets. Beside segmentation, deep-learning based solutions have been exploited for skull-stripping, and tissues identification (white matter, gray matter, etc. . .) [26, 19], At the best of our knowledge, the latest review of radiomics approaches is reported in [12].

### **Topological features for radiomics**

A topological space is a powerful mathematical concept for describing the connectivity of a space. Informally, a *topological space* is a set of points, each of which equipped with the notion of *neighboring* [23, 33]. In the last decade a new suite of tools, based on algebraic topology, for data exploration and modeling haven been invented [9, 57, 16]. The data science community refers to these tools as *Topological Data Analysis* (TDA). TDA has been used in different domains: biology, manufacturing, medicine and others [43]. Topological entropy, namely Persistent Entropy, is equipped with suitable mathematical properties, that permits to describe complex systems [3] and it has been applied in different experiments, e.g. the analysis of biological images [25] and the analysis of medical signals [38]. At the best of our knowledge, the extraction of topological features for radiomics from topological data (TDA) analysis is still at its own infancy. In [37], the authors have compared the accuracy of machine learning models for the classification of hepatic tumors. From T1-weighted magnetic resonance (MR) images, the authors have computed both texture analysis and topological data analysis using persistent homology. The textural features or the topological features were used as input for machine learning models, the best accuracy (92%) for hepatocellular carcinomas was obtained with textural features, while TDA based machine learning model obtained the 85% of accuracy for metastatic tumors. In this work, we report on seminal findings of topological features, computed via topological data analysis, as a new set of features for radiomics purposes. Specifically, we discuss about the application of TDA for GBM detection and segmentation.

## Paper outline

The aim of this study was to evaluate the possibility of discriminating healthy and pathological tissue on FLAIR MR images, by the use of Statistical Texture Analysis and Topological Data Analysis. In fact, FLAIR reveals a wide range of lesions, including cortical, periventricular, and meningeal diseases that were difficult to see on conventional images. Inspired by the paradigm "let the data speak for themselves" introduced in [20] by Gould, We have focused only on textural and topological features, since we believe these are the exact combinatorial representation of what the MDs see when looking at the gray scale images. The discriminating power of statistical texture and of topological features was then exploited for the development of a supervised tumor detection and segmentation methodology by means of automatic and interpretable machine learning algorithms. The paper is organized as follows: in Section 2 we introduce the relevant background, namely the fundamental concepts of *superpixels*, *textural features* and *topological features*. Section 3 introduces the innovative methodologies for GBM detection and segmentation. In Section 4 we report on the implementation and application of the methodologies on slices extracted from public domain FLAIR images. Final thoughts about the results and next steps are discussed in the last Section 5.

## 2 Background

### 2.1 Superpixel

Superpixel is a powerful tool widely adopted in image segmentation. A superpixel is a collection of pixels with common characteristics (e.g., gray scale). For an example of segmentation with superpixels see Figure 2.1. Superpixel enables to extract more information than working at single pixel. Also, each superpixel is a compact representation of image region of interest (ROI) and that can be very useful for computationally demanding problems (e.g., the ease the handling of extremely high resolution images). For a complete overview of superpixel we refer to [24, 54, 1]. In this work, we used the *Simple Linear Iterative Clustering* (SLIC) algorithm for computing superpixels<sup>1</sup>. The algorithm starts with K regularly spaced cluster centers and it moves them to seed locations corresponding to the lowest gradient position in a grid of neighborhood pixels. Each pixel in the image is associated with the nearest cluster center whose search area overlaps this pixel. After all the pixels are associated with the nearest cluster center, a new center is computed as the average color vector of all the pixels belonging

---

<sup>1</sup><https://www.peterkovesi.com/projects/segmentation/> - last visit on 12/4/2019

to the cluster. The process is repeated until all the pixels are associated to the clusters.

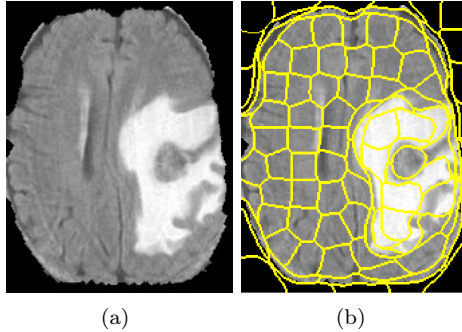


Figure 1: Example of superpixel over-segmentation on skull stripped flair image with 50 superpixels : left - original image; right - original image over-segmented with superpixels.

## 2.2 Gray-Level Co-occurrence matrix

Gray-Level Co-occurrence matrix, often referred as GLCM, is a statistical method on examining image texture by taking into account the spatial relationship of pixels. The GLCM counts how often pairs of pixel with specific values and in a specified spatial relationship occur in an image. From GLCM it is possible to extract textural information, e.g. correlation, energy, homogeneity, etc. . . [21].

## 2.3 Topological Data Analysis

### Persistent homology

Homology is an algebraic machinery used for describing a topological space  $\mathcal{C}$ . Informally, for a fixed natural number  $k$ , the  $k$ -Betti number  $\beta_k$  counts the number of  $k$ -dimensional holes characterizing  $\mathcal{C}$ :  $\beta_0$  is the number of connected components,  $\beta_1$  counts the number of holes in 2D or tunnels in 3D<sup>2</sup>,  $\beta_2$  can be thought as the number of voids in geometric solids, and so on.

Persistent homology is a method for computing the  $k$ -dimensional holes at different spatial resolutions. Persistent holes are more likely to represent true features of the underlying space, rather than artifacts of sampling (noise), or due to particular choices of parameters. For a more formal description we refer the reader to [17]. In order to compute persistent homology, we need a distance function on the underlying space. This can be obtained constructing a *filtration* on a simplicial complex, which is a nested sequence of increasing subcomplexes.

<sup>2</sup>Here  $nD$  refers to the  $n$ -dimensional space  $\mathbb{R}^n$ .

More formally, a filtered simplicial complex  $K$  is a collection of subcomplexes  $\{K(t) : t \in \mathbb{R}\}$  of  $K$  such that  $K(t) \subset K(s)$  for  $t < s$  and there exists  $t_{max} \in \mathbb{R}$  such that  $K_{t_{max}} = K$ . The filtration time (or filter value) of a simplex  $\sigma \in K$  is the smallest  $t$  such that  $\sigma \in K(t)$ .

Persistent homology describes how the homology of  $K$  changes along a filtration. A  $k$ -dimensional Betti interval, with endpoints  $[t_{start}, t_{end})$ , corresponds to a  $k$ -dimensional hole that appears at filtration time  $t_{start}$  and remains until time  $t_{end}$ . We refer to the holes that are still present at  $t = t_{max}$  as *persistent topological features*, otherwise they are considered *topological noise* [2]. Figure 2.3 depicts the computation of persistent homology from a filtered simplicial complex made by four 2-simplices (i.e., filled triangles). The set of intervals representing birth and death times of homology classes is called the *persistence barcode* associated to the corresponding filtration. Instead of bars, we sometimes draw points in the plane such that a point  $(x, y) \in \mathbb{R}^2$  (with  $x < y$ ) corresponds to a bar  $[x, y)$  in the barcode. This set of points is called *persistence diagram*. There are several algorithms for computing persistent barcodes. To name a few: Gudhi and jHoles [32, 8]. For a complete overview of the available tools we refer to [36].

## From image to filtered simplicial complex

We propose a new algorithm for transforming a gray scale image into a filtered simplicial complex. Eventually, the simplicial complex is analyzed by means of persistent homology. The input of the algorithm is a gray scale image or a part of it.

- The image is segmented with  $k$  superpixels, this returns a group of  $k$  superpixel regions:  $S = \{s_1 \dots, s_k\}$  where each superpixel is a group of pixels  $s_1 = \{p_1, \dots, p_n\}$ . We remark that each pixel is described in term of its gray level, namely  $gray(p_i)$ .
- Superpixels became the vertices of a graph  $G = (V \times E)$ ,  $V = \{s_1, \dots, s_n\}$ ,  $E = \{e_{1,2}, \dots, e_{m,n}\}$ . Two nodes are connected if the corresponding superpixels are adjacent. The edge is weighted with  $f(e_{i,j}) = \max\{gray(v_i), gray(v_j)\}$ , where  $gray(v_i)$  is the average gray of the  $i$ th superpixel.
- Persistent homology of the weighted graph is computed by jHoles [8].

## Topological Features for Radiomics

From a persistent barcode it is possible to compute numerical statistics that can be used as input features for further modeling tasks. The main features are recalled in the following.

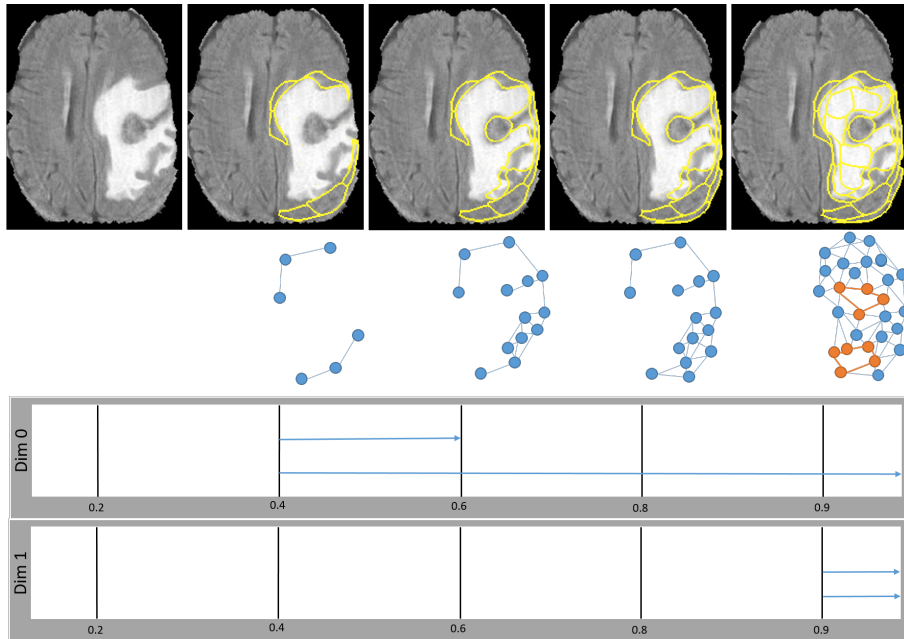


Figure 2: Pictorial representation of computation of persistent homology from a FLAIR slice. The methodology for associating a weighted graph (middle) to the gray scale image by means of adjacent superpixel (top) is fully described in the text. The graph is the skeleton of the filtered the simplicial complex. Persistent homology is computed on the filtered simplicial complex by means of Clique Weight Rank Persistent Homology and it produces the persistent barcodes (bottom). At the beginning ( $t = 0.0$ ) the topological space is empty, once  $t$  increases ( $t = 0.2$ ) two unconnected regions are segmented by the superpixels and thus two sub-graphs (connected components) appear ( $H_0 = 2$ ). For intermediate values of  $t$  ( $0.2 < t < 1.0$ ) the segmentation identifies tissue surrounded by the tumor and the two connected components merge into one ( $H_0 = 1$ ). At  $t = 0.8$  superpixels on the bottom of the image appear, they correspond to tissues with some fat cells. This highlights that the preprocessing might have not removed all the fat. At  $t = 0.9$  (segmentation of the tumor tissue) two loop appear ( $H_0 = 1, H_1 = 2$ ). The red vertices and line segments generating the 1-D holes are called homological generators. Likely, for  $t > 0.9$  the loops disappear and the persistent Betti numbers are ( $H_0 = 1, H_{i>0} = 0$ ).

### Euler Characteristics

Two or more topological objects, e.g. simplicial complexes, are homologically equivalent if they have the same sequence of Betti numbers. In other words, they are characterized by the same number of homological holes at each dimension. Two topological objects can be compared by using their Euler Characteristics.

#### Definition 2.1 (Euler Characteristic)



$$\chi = \sum_{i=0}^{i=n} (-1)^i \beta_i$$

Where  $\beta_i$  is the Betti numbers at the  $i$ -th homological group (e.g.,  $\beta_0$  is the Betti number at  $H_0$  for counting the number of connected componets,  $\beta_1$  for counting the number of 2D holes,  $\beta_2$  for counting the number of 3D empty volumes etc. . . ).

### Persistent Entropy

Persistent Entropy is a Shannon like entropy computed over the persistent barcodes. It was defined initially in [13] and further studies of its mathematical properties were published in [41, 42]. We recall its definition.

#### Definition 2.2 (Persistent Entropy)

Given a filtered simplicial complex  $\{K(t) : t \in F\}$ , and the corresponding persistence barcode  $B = \{a_i = [x_i, y_i) : i \in I\}$ , the Persistent Entropy (PE)  $H$  of the filtered simplicial complex is defined as follows:

$$H = - \sum_{i \in I} p_i \log_{10}(p_i)$$

where  $p_i = \frac{\ell_i}{L}$ ,  $\ell_i = y_i - x_i$ , and  $L = \sum_{i \in I} \ell_i$ .

In the case of an interval with no death time,  $[x_i, +\infty)$ , we truncate infinite intervals and replace  $[x_i, +\infty)$  by  $[x_i, m)$  in the persistence barcode, where  $m = t_{\max} + 1$ .

Note that the maximum PE corresponds to the situation in which all the intervals in the barcode are of equal length. In that case,  $H = \log n$  if  $n$  is the number of elements of  $I$ . Conversely, the value of the PE decreases as more intervals of different length are present.

### Generator Entropy

A topological feature is generated by the so-called *homological generator* [34]. In this work, we propose a new seminal statistics that summarizes the number of 0D generators in each topological features.

#### Definition 2.3 (Generator Entropy)

$$GH = - \sum_{i=1}^{i=N} (p_i \log_{10}(p_i))$$

where  $N$  is the number of homological holes,  $n_i =$  number of unique generators in the  $i$ -th homological hole,  $L = \sum_{i=1}^{i=N} n_i$  and  $p_i = \frac{n_i}{L}$ .

We envision that this new topological statistics could be used for detecting correlations between holes length and specific objects in the input space represented by the simplicial complex (e.g., tumors).

### 3 A new methodology for supervised brain tissue detection and segmentation

#### Methodology for glioblastoma detection

In this work we have implemented and tested the methodology depicted in Figure 3 and that is based on the algorithm described in Sec. 2. The methodology takes as input a collection of FLAIR file. Each FLAIR file is completed with a 3D tumor mask, or in other words with the region of interest (ROI), that indicates where the tumor is located. The methodology counts the following steps:

1. Preprocessing
  - The FLAIR file is optimized by removing fat tissues and by performing skull stripping.
  - Accordingly to the 3D ROI, the slices containing GBM are extracted from the FLAIR file. For each slice the information on the position of the tumor with respect to the center of the image is also stored.
2. Each slice is divided it in two sub-images the so-called lateral and contralateral. In this setting, lateral images contain the tumor, while contralateral images contain healthy tissue. The sub-images are resized such that they have the same sizes.
3. For each sub-image the following statistics are computed:
  - Textural Features - note that, features  $b$  to  $f$  are computed from the GLCM associated to the sub-image:
    - (a) Gray level - average grays intensity in each sub-image.
    - (b) Contrast - it measures the local variability in the gray level.
    - (c) Correlation - it measures the joint probability that a given pair of pixels is found.
    - (d) Homogeneity - it measures the distance between the GCLM diagonal and element distribution.
    - (e) Energy

- Topological features from the simplicial complex associated to the image under analysis:
    - (a) Euler characteristics.
    - (b) Persistent entropy.
    - (c) Generator entropy.
4. Each sub-image is represented by a feature vector of length 8 plus a label :  $l = \{0, 1\}$  if the vector was computed from lateral or controlateral, respectively.
  5. The collection of feature vectors shape the dataset, that is divided randomly in three different subsets: *training*, *testing* and *validation* that contain the 70%, 15% and 15% of samples respectively. We remark that the training set is used for training a machine learning (ML) classifier. The test set is used for improving the tuning of the algorithm and to increase the prediction reliability of the algorithm. The validation set is used for measuring the performances of the trained ML classifier that are reported by receiver operating characteristic curve (ROC) and area under curve (AUC). Selection of ML algorithm can be obtained by using Automatic Machine Learning approach.
  6. Classifier is debugged by tools from information theory that compute both global and local features relevance. This allows to understand the relevance of each feature and to understand what are the numerical input characteristics related to the output.

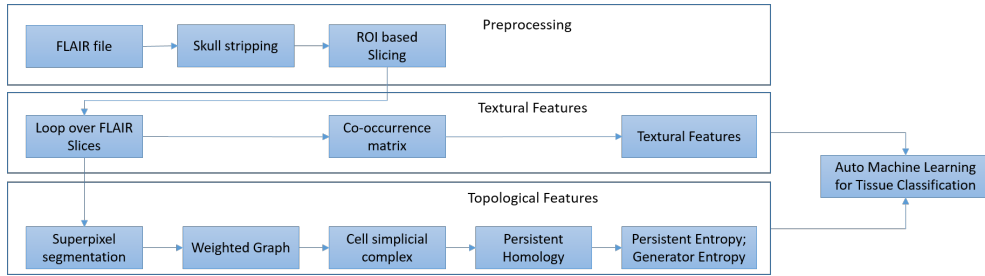


Figure 3: Data analysis workflow presented in this research paper. The pipeline is divided in four main blocks: preprocessing, textural and topological features extraction and finally automatic machine learning for brain tissue classification. Details are reported in the text of Sec. 3.

## Methodology for glioblastoma segmentation

A slightly modified version of the methodology can be used for the segmentation of a slice and without the need of dividing it into lateral and contralateral. After the preprocessing step, the image is initially simplified by superpixels. For each superpixel the textural features and topological features are computed, as described above. The intersection between the pixels in the superpixel regions and the corresponding pixels in the ROI image is computed. If the intersection is  $\emptyset$  the class for superpixel is set to *healthy*, otherwise the class is set to be *ill*.

## 4 Discussion

We have tested the methodology described in Sec. 3 on a public freely available dataset accessible via *The Cancer Imaging Archive (TCIA)* [14]. Fig. 4 shows two of the slices used in this work. In details, the dataset includes DICOM files of 20 subjects from different sites with primary newly diagnosed glioblastoma who were treated with surgery and standard concomitant chemo-radiation therapy (CRT) followed by adjuvant chemotherapy. The sequences are T1-weighted (pre and post-contrast agent), FLAIR, T2-weighted, ADC, normalized cerebral blood flow, normalized relative cerebral blood volume, standardized relative cerebral blood volume, and binary tumor masks (i.e., ROIs) [47, 18]. Each patient is described by two MRI exams: within 90 days following CRT completion and at progression. For the sake of clarity, the dataset was collected for collecting numerical evidences that DSC-MRI perfusion metrics also when recorded from different sites shall be used as complementary data for the assessment of brain tumors. At the best of our knowledge, the dataset was never used for machine or deep learning automatic image classification purposes [46]. We have processed the FLAIR sequences collected within the 90 days of CRT completion and to exclude the follow-up set of images. In the former set the tumor is always present and this gives us the possibility to shape a class-balanced dataset. The DICOMs were transformed into NII files for enabling preprocessing steps<sup>3</sup>. The preprocessing steps, namely the removal of fat tissues and skull stripping, were performed by using the deep-learning algorithm described in [29]<sup>4</sup>. From FLAIR files a total of 2408 gray scale images were extracted. Note that each image contains the tumor.

---

<sup>3</sup><https://pypi.org/project/dicom2nifti/>

<sup>4</sup><https://github.com/JanaLipkova/s3>

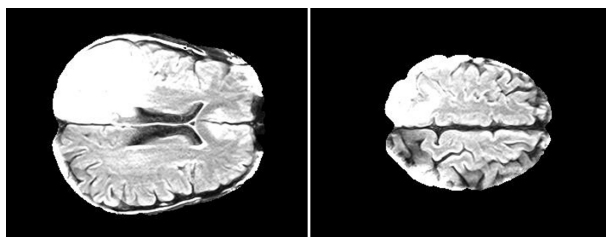


Figure 4: Example of slices contained in the dataset.

## Glioblastoma detection

The images were partitioned in 2408 lateral parts plus 2408 contralateral parts for a total of 4816 samples. Textural and topological features were calculated with open source software Octave<sup>5</sup> and jHoles [8]. The dataset was randomly divided in the training, testing and validation subsets. The dataset was used for two different machine learning experiments. In the first experiment we have trained a multilayer supervised perceptron (MLP)<sup>6</sup> with a fixed architecture of a single hidden layer with 8 neurons each of them equipped with *lbfgs*. The algorithm was trained with the back-propagation approach. In this work the data were preprocessed by applying standard scaler<sup>7</sup>. In the second experiment we used the automatic machine learning framework TPOT [35]. TPOT is a framework that uses genetic algorithm for comparing different machine learning solutions and it finds automatically the best pipeline that maximizes the accuracy. TPOT produces a pipeline that contains both the preprocessing steps - if needed - and the selected Machine Learning architecture. In both experiments and for increasing prediction reliability, 5-fold cross validation<sup>8</sup> approach was used during the training. Skater and Lime algorithms were used for investigating the structure of the trained machine learning algorithms and for computing features relevance<sup>9</sup> [51].

## Glioblastoma segmentation

For evaluating the methodology for glioma segmentation each slice has been segmented in 250 superpixels. The dataset thus contains  $250 \times 2408 = 602.000$  samples. Each sample is completed with its class label, as described in the methodology. Similarly to the methodology for the detection, the dataset was

<sup>5</sup><https://www.gnu.org/software/octave/>

<sup>6</sup>[https://scikit-learn.org/stable/modules/generated/sklearn.neural\\_network.MLPClassifier.html](https://scikit-learn.org/stable/modules/generated/sklearn.neural_network.MLPClassifier.html)

<sup>7</sup><https://scikit-learn.org/stable/modules/generated/sklearn.preprocessing.StandardScaler.html>

<sup>8</sup>[https://scikit-learn.org/stable/modules/cross\\_validation.html](https://scikit-learn.org/stable/modules/cross_validation.html)

<sup>9</sup><https://www.oreilly.com/ideas/interpreting-predictive-models-with-skater-unboxing-model-opacity>

divided in three subsets and used for training and evaluating both a multi layer perceptron and automatic selected machine learning classifier by TPOT.

## Results

### Glioblastoma detection

The methodology described in Sec. 3 was evaluated over different number of superpixels, i.e., from 50 to 500 with an increment of 50. For each number of superpixels we have evaluated the accuracy by means of AUC of both the Artificial Neural Networks and TPOT models. The comparison of the performances is displayed in Figure 4. In general, TPOT model outperforms artificial neural network. TPOT reaches the maximum accuracy at superpixels = 500: TPOT AUC = 97.1% and ANN AUC = 93.7%. Table 1 reports the accuracy and the corresponding 95% confidence interval for each experiment and for both TPOT and ANN. The list of algorithms that were selected by TPOT are reported in Sec.3.

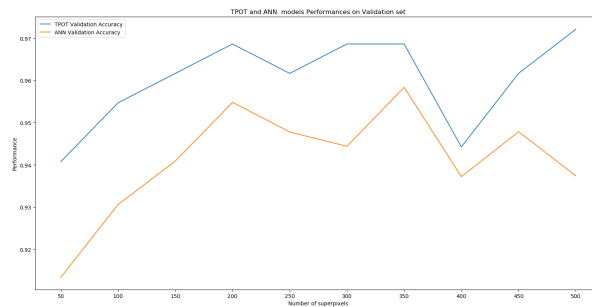


Figure 5: Accuracy comparison on the validation set of both TPOT and ANN accuracy over different number of superpixels.

In both cases the accuracy are quite good. We argue that TPOT shows better performance because it adds preprocessing steps (e.g., StandardScaler<sup>10</sup>, RobustScaler<sup>11</sup> and Normalizer<sup>12</sup>) that increase the separation of the features with respect of the two classes. For the sake of completeness, raw data does not show any strong separation for what concerns the two classes, please see Figure 4.

The analysis of the average feature relevance with respect to the ML algorithm is depicted in Figure 4. For ANN the textural features *gray levels energy*, and

<sup>10</sup><https://scikit-learn.org/stable/modules/generated/sklearn.preprocessing.StandardScaler.html>

<sup>11</sup><https://scikit-learn.org/stable/modules/generated/sklearn.preprocessing.RobustScaler.html>

<sup>12</sup><https://scikit-learn.org/stable/modules/generated/sklearn.preprocessing.Normalizer.html>

Superpixels	ANN		TPOT	
	AUC	95% C. I.	AUC	95% C. I.
50	0.913	[0.858 - 0.969]	0.941	[0.885 - 0.978]
100	0.931	[0.892 - 0.969]	0.955	[0.916 - 0.991]
150	0.941	[0.924 - 0.958]	0.962	[0.932 - 0.993]
200	0.955	[0.933 - 0.977]	0.969	[0.945 - 0.996]
250	0.948	[0.924 - 0.971]	0.962	[0.932 - 0.993]
300	0.944	[0.910 - 0.978]	0.969	[0.945 - 0.996]
350	0.958	[0.930 - 0.987]	0.969	[0.945 - 0.996]
400	0.937	[0.920 - 0.955]	0.969	[0.945 - 0.996]
450	0.948	[0.920 - 0.975]	0.962	[0.932 - 0.993]
500	0.937	[0.898 - 0.977]	0.972	[0.947 - 1.0]

Table 1: Machine learning models accuracy

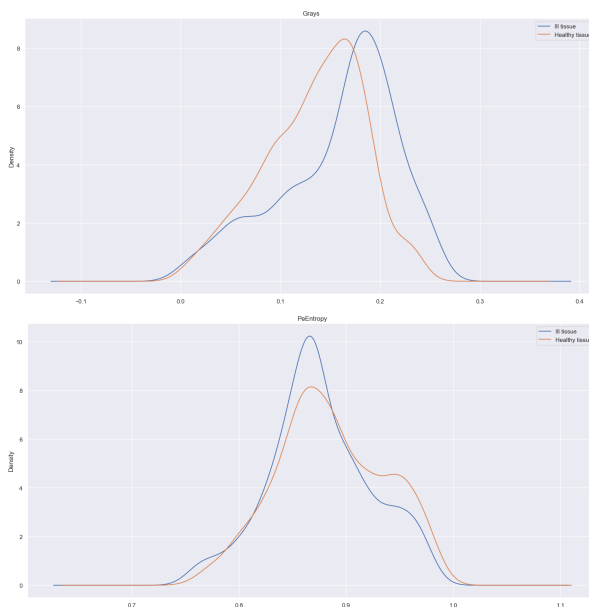


Figure 6: Comparison of density plots for ill and healthy tissues for gray levels (top) and persistent entropy (bottom). For typographic reasons we report only 2 out of 8 density plots.

*homogeneity* are the most informative features. The two topological entropies, namely *Persistent Entropy (PE)* and *Generator Entropy (Gen)* compensate each other. PE is quite important for superpixels = 350 and it corresponds to the point in which the accuracy of the ANN reaches its maximum. For TPOT models the topological features are less important, while textural features *correlation*, *energy* and *contrast* are fundamental.

Lime algorithm allows us to understand what are the numerical characteristic for a patient to be classified healthy or ill, see Figure 4. Positive (blue) indicate

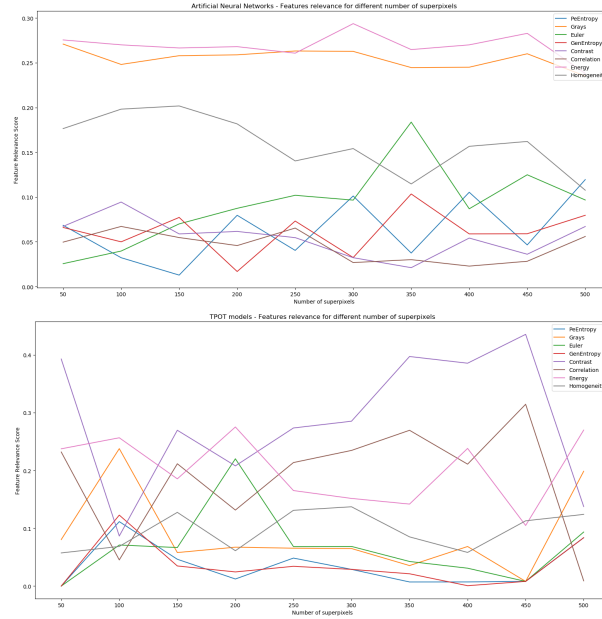


Figure 7: Global analysis of features relevance for ANN (top) and TPOT models (bottom).

ill tissues, while negative (orange) indicate healthy tissue. The way to interpret the weights by applying them to the prediction probabilities. The bars indicate the weight for each feature and the corresponding value for the slice under test. For example, in case of ANN model, a slice to be classified as healthy shall have grays  $> 0.74$ , homogeneity  $\leq -0.37$ , Persistent Entropy  $\leq -.65$ , etc... In case of TPOT model, if we set to zero the values for the features Energy, Contrast and GenEntropy we expect the classifier to predict the slice under test as *ill tissue* with probability  $1.00 - 0.39 - 0.06 - 0.04 = 0.51$  that would mean approximately random detection. This highlights that even if some features might have globally less relevance, they are locally fundamental for avoiding "flipping coin" predictions.

### Glioblastoma segmentation

The methodology for glioblastoma segmentation reported in Sec. 3 was evaluated for a fixed number of superpixels = 250. For the sake of clarity, 250 is a good trade-off between the accuracy, the number of pixels in each superpixel and the timing of the experiments<sup>13</sup>. The accuracy on the validation set of ANN and of TPOT are reported in Table 2. Also for segmentation TPOT outperforms ANN.

<sup>13</sup>Note that, all the numerical experiments were executed on Apple MaBook Air equipped with CPU 1.6GHz, 8GB RAM@1600MHZ, macOS Mojave ver. 10.14.6, Python 3.7.3



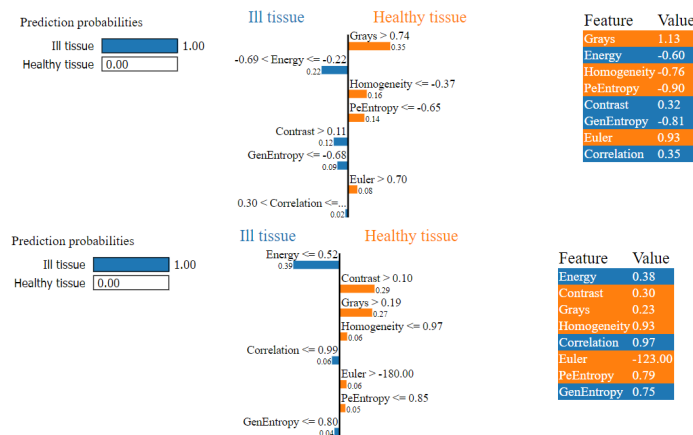


Figure 8: Local analysis of features relevance for ANN (top) and TPOT models (bottom).

	ANN		TPOT	
	AUC	95% C. I.	AUC	95% C. I.
250	0.94	[0.93 - 0.95],	0.95	[0.94 - 0.96]

Table 2: Machine learning models accuracy for the segmentation experiment

An example of the execution of the segmentation is depicted in Fig.4. We argue



Figure 9: Output of the segmentation process. Input image (left) - Detected tumor (right). Yellow indicates the GBM. Green corresponds to internal tissues or other pathologies that are beyond the scope of this paper.

that even in this case the preprocessing steps introduced by TPOT improves the quality of the results. The pipeline selected by TPOT is reported below. Skater analysis is depicted in Fig. 4. The model selected by TPOT for the segmentation task is strongly conditioned by the topological features, while textural features are still the most relevant for the artificial neural network. Lime analysis is reported in Fig. 4. For TPOT the removal of persistent entropy would cause a miss-classification of the superpixel under test.

```
exported_pipeline = make_pipeline(
    MinMaxScaler(),
```

```

StackingEstimator(estimator=KNeighborsClassifier ...
    (n_neighbors=17, p=1, weights="distance")),
KNeighborsClassifier(n_neighbors=1, p=2, ...
    weights="uniform")
)

```

Listing 1: TPOT classifier for segmentation

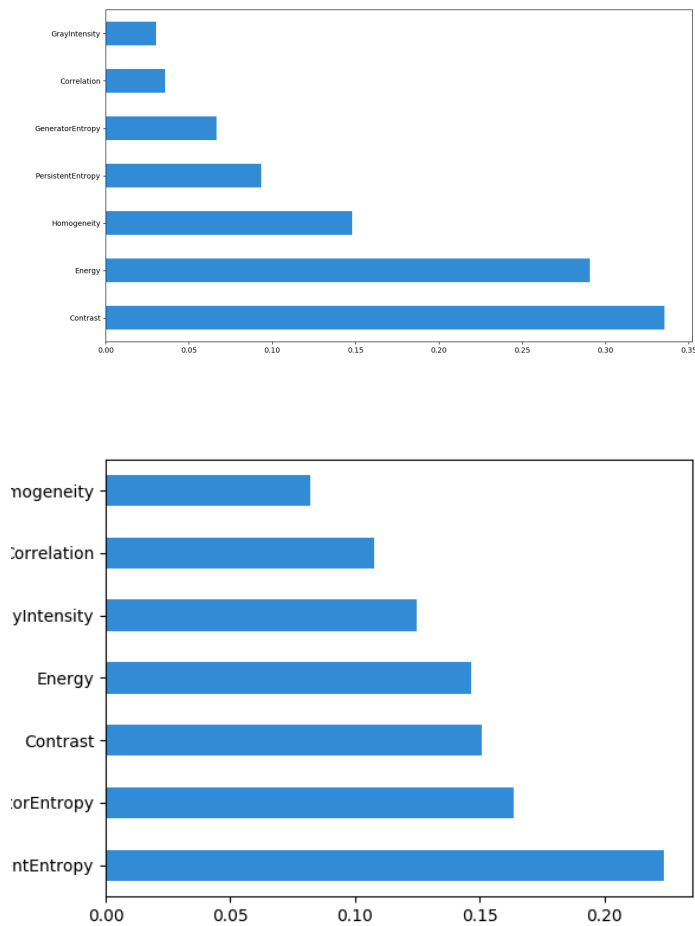


Figure 10: Global analysis of features relevance for ANN (top) and TPOT models (bottom) for the segmentation task.

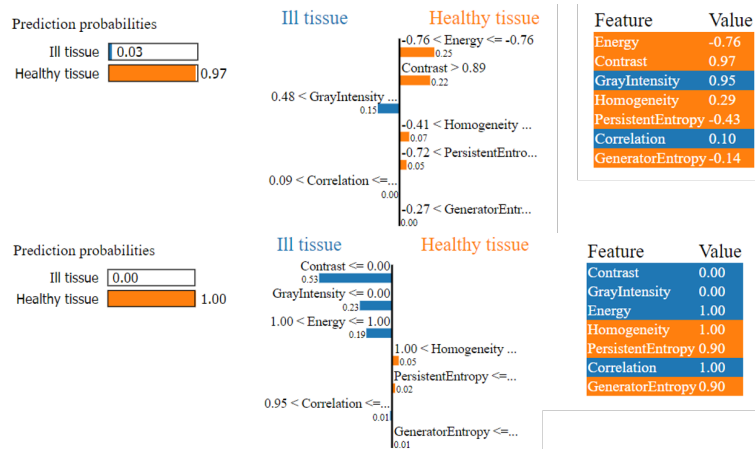


Figure 11: Local analysis of features relevance for ANN (top) and TPOT models (bottom) for the segmentation task.

## GBM detection and segmentation - Performances comparison with deep learning approach

In order to pinpoint out the limitations of our solutions, we have compared them with other public available methods. In particular, since deep-learning based solutions are opening new doors in the field of GBM detection and segmentation, we have challenged the *3D U-Net Convolution Neural Network with Keras* approach [6]. Among the others, the *3D U-net CNN* approach is released with all the information needed for its execution both on the BRATS and other dataset<sup>14</sup>. The model was trained by using both the training dataset described in this text plus other GBM data from TCIA [4]. The accuracy for GBM detection of the *3D U-net CNN* on the same test set used for our ML experiment is  $AUC = 0.982$ , 95% C.I. [0.974 - 1.0]. We remark that the best AUC reached by our approach with TPOT was  $AUC = 0.972$  95% C.I. [0.947 - 1.0]. The quality of the ROIs produced the two approaches by is measured by the Dice coefficient. The Dice coefficient for *3D U-net CNN* is  $D = 0.97$ , while for Topo-ML approach is  $D = 0.91$ . The ROIs produced by *3D U-net CNN* are more precise with respect to the ROIs produced by our approach.

## 5 Conclusions

We have described a method for semi-automatic detection and segmentation of cerebral glioblastomas in brain Flair sequences by means of a classifier trained on statistical texture features and topological features. The use of textural features in

<sup>14</sup><https://github.com/ellisdg/3DUnetCNN>

combination with topological data analysis and interpretable automatic machine learning in FLAIR sequences, with the aim of detecting brain tumor, is, at the best of our knowledge, a new approach. Fast and reliable assessment of glioma presence is critical for an accurate surgical and radiotherapy planning as well as to evaluate and quantify treatment-related effects and progression. In the recent period, surgical approaches are strongly changed, with a progressive shift from classical neurosurgical techniques towards newer approaches with surgical navigation systems, , fluorescence-guided and MR-guided surgery [52, 50, 28]. Also chemotherapy employed techniques with wafer drugs positioning in situ to minimize systemic collateral effects [22]. Consequently, radiological techniques able to localize and evidence every minimum GBM localization are essential to enforce new therapeutic possibilities able to improve the extent of tumor resection, prolong survival and increase the quality of life. Our method started with a procedure for image simplification by means of superpixels segmentation and thorough the characterization of healthy and pathologic tissue by the use of textural and topological features. The features were computed over different number of superpixels. Then, both artificial neural network and automatic machine learning were used to train an automatic supervised classifier. The quality of classification was assessed by ROC curves, and AUC values were indeed quite large (detection: AUC for ANN = 0.96 - 95% C. I. : [0.93 - 0.98] , AUC for TPOT = 0.97 95% C. I. : [0.95 - 1.0]), (segmentation: AUC for ANN = 0.94, 95% CI [0.93, 0.95], AUC for TPOT = 0.95, 95% CI [0.93, 0.96]). The performances were evaluated on a public and freely available dataset. Finally, the trained systems were investigated with tools from information theory. Skater and Lime algorithms allowed to compute features relevance and for understanding what are the numerical characteristics of an input sample to be classified ill or healthy. Among the topological features, we have introduced a new topological entropy, the so-called *generator entropy* that would summarize the role of the length of homological cycles for tissue classification. We have compared the performances of our methods with deep learning based solution. For the sake of completeness, we observed the accuracy of GBM detection is quite the same, while the quality of the ROIs for the segmentation task produced by *3D U-net CNN* (Dice = 0.97) outperforms the ones obtained with our method (D = 0.91). However, we would like to remark that in general Deep Learning based methods require an extremely high number of input samples and ad-hoc hardware for their training. The huge amount of input samples might require an extreme human effort during the annotation of the images (ROIs drawing, labeling, etc...). Also, we noticed that on the PC used for the experiments<sup>15</sup> the segmentation

<sup>15</sup>Note that, all the numerical experiments were executed on Apple MaBook Air equipped with CPU 1.6GHz, 8GB RAM@1600MHZ, macOS Mojave ver. 10.14.6, Python 3.7.3

on the test samples with the Deep-learning solution takes up to 12 minutes per images, while the machine learning solution takes up to 40 seconds per images. Moreover the feature space of the deep learning solution can be presented in some human readable format but its understanding might be unfeasible, since the convolutional features might not correspond to any physical information. In the future, we envision several efforts: we would like to evaluate if the approach described in this paper allows to quantify and to monitor structural changes of the tumor during follow-up period. Eventually, we intend to investigate mathematical properties (minimum set of generators, stability theorem, etc. . .) of the new topological entropy [34]. We intend also to investigate the role of tools for machine learning interpretation for developing a Computer-Aided Detection tool to be compliant with the EU-GDPR 22nd article ("Automated individual decision-making, including profiling") for the "right to be informed"<sup>16</sup>. We intend to combine topological data analysis methods with dynamical system analysis for providing personalized tumor growth models and for comparing the effect of different treatment strategies [40, 56, 7].

## 6 Acknowledgement

The author would like to thank Prof. Rocio Diaz-Gonzalez for the discussions about the role of topological entropy and of homological generators; Prof. Matthias Zeppelzauer for the initial advise on using superpixels for image simplification; Dr. Giorgio De Nunzio, Dr. Marina Donativi and MD Antonella Castellano for long-standing conversations on GBM segmentation. Andrea De Antoni for the discussions on how to improve the presentation of the main findings.

## References

- [1] Radhakrishna Achanta, Appu Shaji, Kevin Smith, Aurelien Lucchi, Pascal Fua, and Sabine Süsstrunk. Slic superpixels. Technical report, 2010.
- [2] Henry Adams and Andrew Tausz. Javaplex tutorial, 2011.
- [3] Nieves Atienza, Rocio Gonzalez-Diaz, and Matteo Rucco. Persistent entropy for separating topological features from noise in vietoris-rips complexes. *Journal of Intelligent Information Systems*, 52(3):637–655, 2019.
- [4] Spyridon Bakas, Hamed Akbari, Aristeidis Sotiras, Michel Bilello, Martin Rozycki, Justin S Kirby, John B Freymann, Keyvan Farahani, and Christos

---

<sup>16</sup><http://www.privacy-regulation.eu/it/22.htm>

- Davatzikos. Advancing the cancer genome atlas glioma mri collections with expert segmentation labels and radiomic features. *Scientific data*, 4:170117, 2017.
- [5] Ron Batash, Noam Asna, Pamela Schaffer, Nicole Francis, and Moshe Schaffer. Glioblastoma multiforme, diagnosis and treatment; recent literature review. *Current medicinal chemistry*, 24(27):3002–3009, 2017.
- [6] Andrew Beers, Ken Chang, James Brown, Emmett Sartor, CP Mammen, Elizabeth Gerstner, Bruce Rosen, and Jayashree Kalpathy-Cramer. Sequential 3d u-nets for biologically-informed brain tumor segmentation. *arXiv preprint arXiv:1709.02967*, 2017.
- [7] Carl M Bender, Ananya Ghatak, and Mariagiovanna Gianfreda. Ptsymmetric model of immune response. *JOURNAL OF PHYSICS A-MATHEMATICAL AND THEORETICAL*, 50(3), 2017.
- [8] Jacopo Binchi, Emanuela Merelli, Matteo Rucco, Giovanni Petri, and Francesco Vaccarino. jHoles: A Tool for Understanding Biological Complex Networks via Clique Weight Rank Persistent Homology. *Electronic Notes in Theoretical Computer Science*, 306:5–18, 2014.
- [9] Gunnar Carlsson. Topology and data. *Bulletin of the American Mathematical Society*, 46(2):255–308, 2009.
- [10] Antonella Castellano, Marina Donativi, Roberta Rudà, Giorgio De Nunzio, Marco Riva, Antonella Iadanza, Luca Bertero, Matteo Rucco, Lorenzo Bello, Riccardo Soffietti, et al. Evaluation of low-grade glioma structural changes after chemotherapy using dti-based histogram analysis and functional diffusion maps. *European radiology*, 26(5):1263–1273, 2016.
- [11] G Castellano, L Bonilha, LM Li, and F Cendes. Texture analysis of medical images. *Clinical radiology*, 59(12):1061–1069, 2004.
- [12] Ahmad Chaddad, Michael Jonathan Kucharczyk, Paul Daniel, Siham Sabri, Bertrand J Jean-Claude, Tamim Niazi, and Bassam Abdulkarim. Radiomics in glioblastoma: current status and challenges facing clinical implementation. *Frontiers in oncology*, 9, 2019.
- [13] Harish Chintakunta, Thanos Gentimis, Rocio Gonzalez-Diaz, Maria-Jose Jimenez, and Hamid Krim. An entropy-based persistence barcode. *Pattern Recognition*, 48(2):391–401, 2015.
- [14] Kenneth Clark, Bruce Vendt, Kirk Smith, John Freymann, Justin Kirby, Paul Koppel, Stephen Moore, Stanley Phillips, David Maffitt, Michael

- Pringle, et al. The cancer imaging archive (tcia): maintaining and operating a public information repository. *Journal of digital imaging*, 26(6):1045–1057, 2013.
- [15] Raymond Damadian. Tumor detection by nuclear magnetic resonance. *Science*, 171(3976):1151–1153, 1971.
- [16] Herbert Edelsbrunner and John Harer. Persistent Homology – a Survey. *Contemporary mathematics*, 453:257–282, 2008.
- [17] Herbert Edelsbrunner and John Harer. *Computational topology: an introduction*. American Mathematical Soc., 2010.
- [18] BM Ellingson, MG Malkin, SD Rand, DP Bedekar, and KM Schmainda. Functional diffusion maps applied to flair abnormal areas are valuable for the clinical monitoring of recurrent brain tumors. In *Proc Intl Soc Mag Reson Med*, volume 17, page 285, 2009.
- [19] Francisco J Galdames, Fabrice Jaillet, and Claudio A Perez. An accurate skull stripping method based on simplex meshes and histogram analysis for magnetic resonance images. *Journal of neuroscience methods*, 206(2):103–119, 2012.
- [20] Peter Gould. Letting the data speak for themselves. *Annals of the Association of American Geographers*, 71(2):166–176, 1981.
- [21] Robert M Haralick, Karthikeyan Shanmugam, and Its’ Hak Dinstein. Textural features for image classification. *IEEE Transactions on systems, man, and cybernetics*, (6):610–621, 1973.
- [22] Michael G Hart, Robert Grant, Ruth Garside, Gabriel Rogers, Margaret Somerville, and Ken Stein. Chemotherapeutic wafers for high grade glioma. *Cochrane Database of Systematic Reviews*, (3), 2008.
- [23] Allen Hatcher. *Algebraic Topology*. Cambridge University Press, 2002.
- [24] Peter W Hawkes. *Advances in imaging and electron physics*, volume 133. Elsevier, 2004.
- [25] María José Jimenez, Matteo Rucco, P Vicente-Munuera, P Gómez-Gálvez, and Luis M Escudero. Topological data analysis for self-organization of biological tissues. In *International Workshop on Combinatorial Image Analysis*, pages 229–242. Springer, 2017.

- [26] Jens Kleesiek, Gregor Urban, Alexander Hubert, Daniel Schwarz, Klaus Maier-Hein, Martin Bendszus, and Armin Biller. Deep mri brain extraction: a 3d convolutional neural network for skull stripping. *NeuroImage*, 129:460–469, 2016.
- [27] Panagiotis Korfiatis, Timothy L Kline, and Bradley J Erickson. Automated segmentation of hyperintense regions in flair mri using deep learning. *Tomography*, 2(4):334, 2016.
- [28] Daniela Kuhnt, Andreas Becker, Oliver Ganslandt, Miriam Bauer, Michael Buchfelder, and Christopher Nimsky. Correlation of the extent of tumor volume resection and patient survival in surgery of glioblastoma multiforme with high-field intraoperative mri guidance. *Neuro-oncology*, 13(12):1339–1348, 2011.
- [29] Jana Lipková, Panagiotis Angelikopoulos, Stephen Wu, Esther Alberts, Benedikt Wiestler, Christian Diehl, Christine Preibisch, Thomas Pyka, Stephanie E Combs, Panagiotis Hadjidakas, et al. Personalized radiotherapy design for glioblastoma: Integrating mathematical tumor models, multimodal scans, and bayesian inference. *IEEE transactions on medical imaging*, 38(8):1875–1884, 2019.
- [30] Pablo Ribalta Lorenzo, Jakub Nalepa, Barbara Bobek-Billewicz, Pawel Wawrzyniak, Grzegorz Mrukwa, Michal Kawulok, Pawel Ulrych, and Michael P Hayball. Segmenting brain tumors from flair mri using fully convolutional neural networks. *Computer methods and programs in biomedicine*, 176:135–148, 2019.
- [31] Carles Majós, Mònica Cos, Sara Castañer, Miguel Gil, Gerard Plans, Anna Lucas, Jordi Bruna, and Carles Aguilera. Early post-operative magnetic resonance imaging in glioblastoma: correlation among radiological findings and overall survival in 60 patients. *European radiology*, 26(4):1048–1055, 2016.
- [32] Clément Maria, Jean-Daniel Boissonnat, Marc Glisse, and Mariette Yvinec. The gudhi library: Simplicial complexes and persistent homology. In *International Congress on Mathematical Software*, pages 167–174. Springer, 2014.
- [33] James R Munkres. *Elements of algebraic topology*, volume 2. Addison-Wesley Reading, 1984.
- [34] Ippei Obayashi. Volume-optimal cycle: Tightest representative cycle of a generator in persistent homology. *SIAM Journal on Applied Algebra and Geometry*, 2(4):508–534, 2018.



- [35] Randal S Olson and Jason H Moore. Tpot: A tree-based pipeline optimization tool for automating machine learning. In *Automated Machine Learning*, pages 151–160. Springer, 2019.
- [36] Nina Otter, Mason A Porter, Ulrike Tillmann, Peter Grindrod, and Heather A Harrington. A roadmap for the computation of persistent homology. *EPJ Data Science*, 6(1):17, 2017.
- [37] Asuka Oyama, Yasuaki Hiraoka, Ipei Obayashi, Yusuke Saikawa, Shigeru Furui, Kenshiro Shiraishi, Shinobu Kumagai, Tatsuya Hayashi, and Jun-ichi Kotoku. Hepatic tumor classification using texture and topology analysis of non-contrast-enhanced three-dimensional t1-weighted mr images with a radiomics approach. *Scientific Reports*, 9(1):8764, 2019.
- [38] Marco Piangerelli, Matteo Rucco, Luca Tesei, and Emanuela Merelli. Topological classifier for detecting the emergence of epileptic seizures. *BMC research notes*, 11(1):392, 2018.
- [39] Fabio Remondino and Sabry El-Hakim. Image-based 3d modelling: a review. *The photogrammetric record*, 21(115):269–291, 2006.
- [40] Tiina Roose, S Jonathan Chapman, and Philip K Maini. Mathematical models of avascular tumor growth. *SIAM review*, 49(2):179–208, 2007.
- [41] Matteo Rucco, Filippo Castiglione, Emanuela Merelli, and Marco Pettini. Characterisation of the idiotypic immune network through persistent entropy. In *Proceedings of ECCS 2014*, pages 117–128. Springer, 2016.
- [42] Matteo Rucco, Rocio Gonzalez-Diaz, Maria-Jose Jimenez, Nieves Atienza, Cristina Cristalli, Enrico Concettoni, Andrea Ferrante, and Emanuela Merelli. A new topological entropy-based approach for measuring similarities among piecewise linear functions. *Signal Processing*, 134:130–138, 2017.
- [43] Matteo Rucco, Adane Letta Mamuye, Marco Piangerelli, Michela Quadrini, Luca Tesei, and Emanuela Merelli. Survey of topdrim applications of topological data analysis. In *CEUR Workshop Proceedings*, volume 1748, page 1814, 2016.
- [44] Lothar R Schad, Stefan Blüml, and Ivan Zuna. Ix. mr tissue characterization of intracranial tumors by means of texture analysis. *Magnetic resonance imaging*, 11(6):889–896, 1993.
- [45] Kubben PL ter Meulen KJ Schijns. Oe ter laak-poort mp van overbeeke jj van santbrink h: Intraoperative mri-guided resection of glioblastoma multiforme: a systematic review. *Lancet Oncol*, 12:1062–1070, 2011.

- [46] Kathleen M Schmainda, Melissa A Prah, Scott D Rand, Ying Liu, Brent Logan, Mark Muzi, Swati D Rane, Xiao Da, Yi-Fen Yen, Jayashree Kalpathy-Cramer, et al. Multi-site concordance of dsc-mri analysis for brain tumors: Results of a nci quantitative imaging network collaborative project. *AJNR. American journal of neuroradiology*, 39(6):1008, 2018.
- [47] Prah M. Schmainda KM. Data from brain tumor progression. the cancer imaging archive. <http://doi.org/10.7937/K9/TCIA.2018.15quzvnv>, 2018.
- [48] Shiv Naresh Shivhare and Nitin Kumar. Brain tumor detection using manifold ranking in flair mri. In *Proceedings of ICETIT 2019*, pages 292–305. Springer, 2020.
- [49] Mohammadreza Soltaninejad, Guang Yang, Tryphon Lambrou, Nigel Allinson, Timothy L Jones, Thomas R Barrick, Franklyn A Howe, and Xujiong Ye. Automated brain tumour detection and segmentation using superpixel-based extremely randomized trees in flair mri. *International journal of computer assisted radiology and surgery*, 12(2):183–203, 2017.
- [50] Walter Stummer, Uwe Pichlmeier, Thomas Meinel, Otmar Dieter Wiestler, Friedhelm Zanella, Hans-Jürgen Reulen, ALA-Glioma Study Group, et al. Fluorescence-guided surgery with 5-aminolevulinic acid for resection of malignant glioma: a randomised controlled multicentre phase iii trial. *The lancet oncology*, 7(5):392–401, 2006.
- [51] Pengfei Wei, Zhenzhou Lu, and Jingwen Song. Variable importance analysis: a comprehensive review. *Reliability Engineering & System Safety*, 142:399–432, 2015.
- [52] M Weller, M Van den Bent, K Hopkins, JC Tonn, R Stupp, A Falini, E Cohen-Jonathan-Moyal, D Frappaz, R Henriksson, C Balana, et al. European association for neuro-oncology (eano) task force on malignant glioma. eano guideline for the diagnosis and treatment of anaplastic gliomas and glioblastoma. *Lancet Oncol*, 15(9):e395–e403, 2014.
- [53] Yaping Wu, Zhe Zhao, Weiguo Wu, Yusong Lin, and Meiyun Wang. Automatic glioma segmentation based on adaptive superpixel. *BMC medical imaging*, 19(1):1–14, 2019.
- [54] F Xing and L Yang. Machine learning and its application in microscopic image analysis. In *Machine Learning and Medical Imaging*, pages 97–127. Elsevier, 2016.

- [55] Zhe Zhao, Guan Yang, Yusong Lin, Haibo Pang, and Meiyun Wang. Automated glioma detection and segmentation using graphical models. *PloS one*, 13(8):e0200745, 2018.
- [56] Bartosz Zielinski, Mateusz Juda, and Matthias Zeppelzauer. Persistence codebooks for topological data analysis. *arXiv preprint arXiv:1802.04852*, 2018.
- [57] Afra Zomorodian. Topological data analysis. In *Advances in Applied and Computational Topology. Proceedings of Symposia in Applied Mathematics*, volume 70, pages 1–39, 2007.

## Appendix

Number of Superpixels	TPOT Model
50	<i>exported_pipeline = make_pipeline(DecisionTreeClassifier(criterion = "entropy",</i>
100	<i>exported_pipeline = make_pipeline(PCA(iterated_power = 8, svd_solver = "l</i>
150	<i>exported_pipeline = make_pipeline(RobustScaler(), StackingEstimator(estim</i>
200	<i>exported_pipeline = make_pipeline(StackingEstimator(estimator = Logistic</i>
250	<i>exported_pipeline = make_pipeline(RobustScaler(), KNeighborsClassifier(n</i>
300	<i>exported_pipeline = make_pipeline(StandardScaler(), RobustScaler(), Norma</i>
350	<i>exported_pipeline = make_pipeline(RobustScaler(), KNeighborsClassifier(n</i>
400	<i>exported_pipeline = DecisionTreeClassifier(criterion = "entropy", max_dep</i>
450	<i>exported_pipeline = make_pipeline(RobustScaler(), KNeighborsClassifier(n</i>
500	<i>exported_pipeline = make_pipeline(StandardScaler(), KNeighborsClassifier</i>

Table 3: Machine learning models selected by TPOT. TPOT produces pipelines by using Scikit-Learn API.